Determining the role of Tubulin Posttranslational Modifications on Axonal Transport

Satish Bodakuntla, Maria M. Magiera, Carsten Janke

Determining the role of tubulin posttranslational modifications on axonal transport

Satish Bodakuntla[1,2], Maria M. Magiera[1,2]* and Carsten Janke[1,2]*

[1]Institut Curie, PSL Research University, CNRS UMR3348, F-91405 Orsay, France

[2]Université Paris Sud, Université Paris-Saclay, CNRS UMR3348, F-91405 Orsay, France

*Corresponding authors:

Maria M. Magiera and Carsten Janke, Institut Curie, PSL Research University, CNRS UMR3348, Centre Universitaire, Bâtiment 110, F-91405 Orsay, France

Carsten.Janke@curie.fr

Maria.Magiera@curie.fr

Running title: Tubulin posttranslational modifications in axonal transport

Abstract:

Axonal transport is a process essential for neuronal function and survival that takes place on the cellular highways – the microtubules. It requires three major components: the microtubules that serve as tracks for the transport, the motor proteins that drive the movement, and the transported cargoes with their adaptor proteins. Axonal transport could be controlled by tubulin posttranslational modifications, which by decorating specific microtubule tracks could determine the specificity of cargo delivery inside neurons. However, it appears that the effects of tubulin modifications on transport can be rather subtle, and might thus be easily overlooked depending on which parameter of the transport process is analysed. Here we propose an analysis paradigm that allows detecting rather subtle alterations in neuronal transport, as induced for instance by accumulation of posttranslational polyglutamylation. Analysing mitochondria movements in axons, we found that neither the average speed nor distance travelled were affected by hyperglutamylation, but we detected an about 50% reduction of the overall motility, suggesting that polyglutamylation controls the efficiency of mitochondria transport in axons. Our protocol can readily be expanded to the analysis of the impact of other tubulin modifications on the transport of a range of different neuronal cargoes.

Key words:

Axonal transport, mitochondria, cargo, microtubules, posttranslational modifications of tubulin, polyglutamylation

1. Introduction

Intracellular transport is an essential process for all eukaryotic cells, as it allows to deliver organelles, mRNA and proteins to their predestined locations in different cellular compartments [1]. The complex morphology of neurons (very long and ramified axons and many dendrites) is particularly challenging for the intracellular transport machinery, which has to work efficiently and adapt to varying physiological requirements throughout the entire life span of an organism. In particular axonal transport, which can cover long distances, needs to be stringently controlled [2]. Defects in axonal transport have been linked to many neurodegenerative disorders, and are suspected to be one of the early molecular defects in many of them [3-5]. One of the key mechanisms to control microtubule properties, and their interactions with molecular transport machineries are posttranslational modifications (PTMs) of tubulins – the building blocks of microtubules [6].

Neuronal microtubules are highly enriched with a variety of tubulin PTMs such as acetylation, detyrosination, and polyglutamylation [7]. Polyglutamylation is a particularly complex PTM, as it can generate branch-chains of variable numbers of glutamate residues selectively on α- or β-tubulin. Thus, polyglutamylation can potentially encode a large variety of information into one and the same microtubule [6]. The signals generated by polyglutamylation are determined by the specificity of the modifying [8,9] and demodifying enzymes [10,11], which in turn can be regulated by cell-type specific expression, subcellular localisation, as well as by adapting the cellular response to external cues [12]. While little is so far known on how polyglutamylation is regulated by signalling pathways, it has been shown that the major polyglutamylases in neurons are TTLL1 and TTLL7 [13,8], and the key deglutamylases are CCP1 and CCP6 [10,14].

Deregulation of tubulin PTMs in cells can result in microtubule dysfunctions and eventually in disease conditions [15]. Indeed, analyses of several mouse models have demonstrated that aberrations in the levels of tubulin polyglutamylation are linked to cilia-related disorders, such as respiratory problems [16], defects in spermatogenesis [17-19] and sperm motility [20], retinal degeneration [21], or neurodegeneration [14,10,22,23].

Mutation or loss of CCP1, one of the major neuronal deglutamylases, leads to unopposed, and thus accumulating polyglutamylation, which results in degeneration of several neuronal populations in the brain, the most emblematic being Purkinje cells [18,10,14]. Strikingly in these mice, some parts of the brain do not degenerate, nor show signs of increased

polyglutamylation. We showed that this was due to the compensation by a second deglutamylase, Ccp6, which was selectively expressed in cerebral cortex and hippocampus, thus protecting these brain regions [14]. These findings were the first to indicate that cell-specific expression of enzymes involved in polyglutamylation can result in cell-specific functions, or defects.

Despite first insights in a widespread implication of tubulin polyglutamylation in pathological conditions [15], underlying molecular mechanisms remained largely elusive, primarily because of a number of technical limitations. These limitations are exemplified when studying sensitive biological processes such as axonal transport. Although there are reports linking transport changes to polyglutamylation [24-26], the direct role of polyglutamylation in controlling transport in neurons has only been recently addressed on primary neurons of the now-available knockout mouse models. One study measured axonal transport in cerebellar granule cells from *ccp1*$^{-/-}$ mice, as the cerebellum is the most affected brain region in this mouse model [22]. In order to determine the impact of increased polyglutamylation in hippocampal neurons, we developed a specific approach to convert *Ccp1*$^{flox/flox}$*Ccp6*$^{flox/flox}$ neurons into *ccp1*$^{-/-}$*ccp6*$^{-/-}$ in the culture dish (cite flox protocol paper here). Measuring axonal transport of mitochondria, we found clear aberrations, however, only one parameter - the overall motility of these organelles – was affected. This could have easily been overlooked when analysing only the motile mitochondria, which is why we used a paradigm that included all mitochondria, even the non-motile ones [14].

Here we describe our procedure for imaging axonal transport in neurons with altered tubulin PTMs, as well as our analysis paradigm to apprehend a range of different, potentially subtle changes in axonal transport. As an example, we show the impact of increased polyglutamylation on the mitochondrial transport. This method can be readily extended to study the transport of other cellular cargoes, and different tubulin PTMs.

Development of the analysis paradigm

One way to study axonal transport is to follow selected, single particles throughout the imaging period, and determine their complex movement behaviour (e.g. overall displacement, frequency of changes in direction, mean anterograde and retrograde speed, etc.). However, some cargoes, such as mitochondria or endosomes, are very dense in axons, making it difficult to reliably track the entire path of every moving particle throughout the imaging period. Analysing only the ‘trackable’ particles, however, can introduce an unwanted bias in the study.

To avoid this, we based our analyses paradigm on previously published work [27,28], analysing individual "runs", rather than tracing the movement of single particles throughout the imaging period. A "run" is defined as an uninterrupted, unidirectional motility event at constant speed. Thus, a change in the speed of a moving particle marks the beginning of a new run (**Fig. 1**). While this analysis paradigm does not inform us on the complex movement of single particles (changes between anterograde and retrograde movements, final destination of a particle), it provides unbiased, statistically exploitable data for parameters that might be altered by tubulin PTMs for both, anterograde and retrograde transport: the speed at which a transport cargo moves along differentially modified microtubules, or its persistence (how long a particle moves before stopping). By taking into account the total number of particles in the field of observation, we can further determine the overall motility within the particle population, thus also taking into account all the non-motile particles in the imaged axon.

Using this analysis paradigm, we investigated the impact of abnormally increased polyglutamylation on axonal transport in hippocampal neurons at DIV4 (4 days in vitro) (cite our other method paper here). In neurons with hyperglutamylated microtubules, both, average speed and time of single runs were unaltered in both, anterograde and retrograde direction, while the overall motility of mitochondria was reduced to about 50% of the control [14] (see **Fig. 4**). This effect could not have been discovered with an approach focusing on tracing only motile mitochondria. We therefore believe that our paradigm for axonal-transport analysis can be used in a broader range of applications, especially when studying subtle changes such as those induced by tubulin PTMs [14].

2. Materials

2.1 Imaging of Axonal Transport

1. CO_2 Testing Equipment (Thermo Scientific™ #50121515)
2. Thermometer
3. Primary mouse hippocampal neurons with normal and modified microtubules cultured on 35-mm glass bottom dishes (Ibidi #81158).
4. B27 medium: For 100 ml, add 2 ml of 50× B27 solution (Thermo Fisher #17504044), 1 ml of 100× Glutamax (Thermo Fisher #35050038) and 1 ml of 100× Penicillin-Streptomycin (Life Technologies #15140130) to 96 ml of plain Neurobasal medium (Thermo Fisher #21103049).
5. Conditioned medium: B27 medium incubated with neurons from DIV0, which is not only equilibrated with the cell culture incubator's atmosphere but importantly with any signalling/growth molecules released by the neurons in to the medium. See (other method paper to cite) for preparing conditioned medium.
6. Nikon Ti-E spinning disk inverted confocal laser microscope equipped with a 60× oil immersion objective (N.A. 1.40) and an ORCA-Flash 4.0 camera (Hamamatsu) controlled through MetaMorph software.
7. 1 mM MitoTracker™ Red CMXRos (Thermo Fisher #M7512): Dissolve 50 µg of MitoTracker™ in 94 µl of Dimethyl Sulfoxide (DMSO) (Sigma #D8418). Aliquot by 10 µl and store at -20°C. Avoid repeated cycles of freeze-thaw.

2.2 Analysis of Axonal Transport

1. ImageJ 1.47v equipped with 'nd Stack Builder' and 'KymoToolBox' plugins.
2. Microsoft Excel and GraphPad Prism or equivalent software to plot and statistically test the obtained data.

3. Methods

In the current protocol, we describe general criteria to follow during the imaging of axonal transport and the analysis paradigm we developed to characterize the transport in neurons in which tubulin PTMs are modulated **(Figs. 1, 2)**. Using this method, we have analysed the mitochondria transport in neurons with normal and abnormally increased polyglutamylation [14]. To obtain primary neurons with increased polyglutamylation, we developed a cell-culture based system, in which primary neurons are isolated from *Ccp1*$^{flox/flox}$*Ccp6*$^{flox/flox}$ mice, and subsequently transduced with either a GFP-encoding (control), or a GFP-2A-*cre*-recombinase encoding lentivirus (to induce the knockout of the two deglutamylases and induce hyperglutamylation) (cite other method article).

We analysed mitochondria transport using the commercially available dye, MitoTracker^{TM}. On DIV4, mitochondrial movements were recorded in the GFP-expressing neurons for 1 min, and subsequently converted to kymographs and analysed using the 'KymoToolBox' plugin [29] for ImageJ [30]. When re-drawing the particle movements in the kymographs, we separately assigned each uninterrupted movement (defined by a constant speed = slope in the kymograph) as one "run" **(Figs. 1, 3)**. Displacement events of less than 0.10 μm/s were considered as immotile.

For each single experiment **(Figs. 1, 4a-e)**, we analysed the distribution of run speed and run time for both, anterograde and retrograde transport. Based on the total amount of particles in the field of observation, we then determined the overall motility of the particle population. Of all the parameters measured, only the overall motility of the mitochondria was strongly decreased in neurons with hyperglutamylation, as compared to control cells **(Fig. 4)** [14].

To exclude that the expression of cre recombinase in the neurons affects the transport, we performed an equivalent set of experiments in wild-type neurons. We demonstrated that the expression of GFP-2A-*cre* did not affect any of the previously measured parameters of mitochondrial transport, thus demonstrating that the decrease of motility in *Ccp1*$^{flox/flox}$*Ccp6*$^{flox/flox}$ neurons transduced with GFP-2A-*cre* was indeed a result of the knockout of the two deglutamylases, and thus of the microtubule hyperglutamylation it induced [14].

3.1 Imaging of Axonal Transport

1. Before starting the experiment use a thermometer and CO_2-testing device to manually verify the temperature and CO_2 levels of the microscope imaging chamber. If needed, calibrate the device such that the imaging stage is at 37°C and 5% CO_2. see **Note 1**.
2. On the day of imaging, remove the medium from the glass-bottom dishes and gently wash the transduced neurons with conditioned medium to remove any remains of the lentivirus from the dish. Pipette the medium gently, always against the edge of the dish and never directly on the neurons. See **Note 2**.
3. Thaw an aliquot of 1 mM MitoTracker™ solution (main stock). Prepare an intermediate 2 µM stock solution by adding 1 µl of the main stock to 500 µl of PBS.
4. Dilute the intermediate stock solution to a final concentration of 2 nM MitoTracker™ by adding 1 µl of 2 µM intermediate stock solution to 1 ml of conditioned medium.
5. Remove the neurobasal culture medium from the dish and quickly, yet gently add 1 ml of conditioned medium containing 2 nM of MitoTracker™. Leave the dish in the incubator for 1 min. See **Note 3**.
6. Remove the medium containing MitoTracker™ and gently wash the neurons with 500 µl of conditioned medium to get rid of any unbound MitoTracker™ dye. Finally, add 1 ml of conditioned medium to the neurons and bring them to the microscope chamber for live imaging.
7. Image neurons immediately using a Nikon Ti-E spinning disk inverted confocal laser microscope equipped with a 60× oil immersion objective (N.A 1.40) and an ORCA-Flash4.0 camera (Hamamatsu), set at 2×2 binning operated by Leica MM AF imaging software. See **Note 4**.
8. After the imaging stage is set, focus on the neurons using bright-field light. DO NOT USE the laser to prevent photobleaching and damaging the neurons.
9. Once the neurons are in focus, use bright-field to find a suitable neuron and identify the axon by its typical characteristics – the longest neurite extending from the cell body. Dendrites at DIV4 are much shorter and thicker compared to axons **(Fig. 2).** See **Note 5**.
10. If it is not possible to capture the cell body and axon in the image, write down the position of the cell body, and its distance from the actual imaging area.

11. Switch to laser fluorescence and verify that the chosen neuron is GFP-positive. Change the excitation wavelength (in the case of MitotrackerTM Red CMXRos) and bring the transport particles in focus. See **Note 6**.

12. Set the gain or intensity of laser to a minimal value at which the transport particles are still clearly visible. Keep the laser settings constant for imaging all neurons in a single experiment. See **Note 7**.

13. Record the particle movements in the axon in streaming mode every 300 ms for a total of 1 min. see **Note 8**.

14. Acquire differential interference contrast (DIC) and GFP-fluorescence image of the axon used for imaging transport to assess the general appearance of the neuron, which can eventually give some indications on the health of the neuron.

15. For the settings we use, acquisition of each neuron will generate one DIC image of the neuron, one image of the GFP expression in the cell, 201 time-lapse images corresponding to 201 time frames of the movie, and one '.nd' file.

16. For each dish, image a minimum of five neurons, however we prefer to image around ten neurons if possible. This is important as the dynamics of axonal transport are inherently heterogenous among individual neurons in culture, and can furthermore be affected by small variations in the experimental conditions.

17. Image each dish for no more than 30 min, as constant laser exposure is deleterious to the neurons.

3.2 Analysis of Axonal Transport

We recommend creating a separate folder for each analysed neuron and saving there all the files generated during the different steps of analysis. In this example, we assume that the name of the cell and the folder is 'Name'.

1. Open the 'Name.nd' MetaMorph file in the ImageJ software by drag-dropping the file on the ImageJ icon or toolbar to visualize the tiff images of the corresponding movie **(Fig. 3a).** In the 'Bio-formats Import Options' window, select view stack with 'hyperstack' and uncheck all other options. See **Note 9**.

2. Calibrate the hyperstack by using 'Image > Properties' menu in ImageJ. Unit of length for defining pixel size is μm and for the frame interval time is seconds. If ImageJ

automatically calibrates the hyperstack, confirm that the values are correct. See **Note 10**.

3. Save the file as 'Name_stack.tiff' in its dedicated folder **(Fig. 3a)**. Once the stack file is generated and saved, the individual files corresponding to all the timepoints of the movie (Name-t0.tiff – Name-t201.tiff) and the corresponding 'Name.nd' file can be deleted.

4. Create a maximum intensity projection of the tiff stack file by using 'Image > Stacks > Z Project'. Subsequently, select 'projection type' as maximum, and start slice and stop slice as 1 and 201, respectively **(Fig. 3b)**.

5. Select the 'segmented line' or 'freehand' line tool and manually identify the axon, in which the cargo movement will be quantified **(Fig. 3c)**. If needed, adjust the intensity of the maximum projection image beforehand (by using 'Image > Adjust > Brightness/Contrast') to better visualize the axon. As a general rule, always trace the axon from the cell body towards the axonal terminal (proximal – distal). See **Note 11**.

6. Add the traced path of the axon to 'ROI manager' by pressing 't'. Save the ROI as 'Name_axon.roi' by using 'More >> save' option.

7. Close the maximum intensity projection image and apply the ROI to the 'Name_stack.tiff' file.

8. Use the 'KymoToolBox' by selecting 'Plugins > KymoToolBox > Draw Kymo' menu to generate the kymograph and the kymostack of the movement in the selected axon. Define the 'Width' as 15 pixels (for the width of identified axon in step 5) and select 'Get kymo' and 'Get kymoStack' **(Fig. 3d)**. The kymograph represents particle movement in time vs. space, while the kymostack generates a straightened movie of the identified axon, which can be later helpful in the identification of particle's movement. Refer to 'https://github.com/fabricecordelieres/IJ_KymoToolBox' for detailed description of the plugin. See **Note 12**.

9. Save the generated kymograph and kymostack as 'Kymograph from Name_stack.tif' and 'Kymostack from Name_stack.tif', respectively in the dedicated folder.

10. On the kymograph, trace all possible individual runs **(Fig. 3e)** of the particle trajectories. If necessary use the kymostacks to help identifying the trajectories. Add each tracing to the 'ROI manager' by pressing 't'. To keep track of the traced

trajectories, select ‘Show All’ on ‘ROI manager’. Save all the ROIs as ‘Name_stack_kymo.zip’ file in the dedicated folder. See **Note 13**.

11. Select ‘Plugins > KymoToolBox > Analyse Kymo’ to retrieve the parameters of each run. Select ‘Outward is’ as ‘From left to right’ and ‘Line width’ as 3 (line width for representation of colour-coded runs). Set ‘Lim. speed’ as 0.10 µm/sec – runs with speed lower than 0.10 µm/sec are considered immotile. Select ‘Log all data’ and ‘Show colored kymo’ to generate a table with the values of movement parameters of trajectories traced in step 10 and a colour-coded kymograph **(Fig. 3f)**. As this analysis paradigm focuses on individual runs, use the data highlighted in yellow, which correspond to individual runs with constant speed and direction, and discard the data highlighted in grey, which correspond to summary of several runs. For the same reason, we only use run length (Cum_Dist), run speed (Mean_Speed) and run duration (Ttl_Time) parameters for further analysis **(Fig. 3f, red box)**. Immotile trajectories are shown as vertical lines in blue while motile trajectories (runs) were shown as diagonal lines (green for anterograde and red for retrograde).

12. Save the colour-coded kymograph as ‘Tracks from kymograph from Name_stack.tiff’ and the results table as ‘Results_Name.xls’ in the dedicated folder.

13. Use the ‘Kymograph from Name_stack.tif’ to determine the number of particles and the length of the axon (in µm) used for analysis **(Fig. 3g)**. See **Note 14**.

14. To calculate one of the parameters to be analysed, the particle density (mitochondria, vesicles) in the axons, use the following equation:

$$Density\ of\ particles\ [/100\ \mu m\ of\ axon] = \frac{Number\ of\ particles\ \times\ 100}{Length\ of\ analysed\ axon\ [\mu m]}$$

15. Repeat steps 1 to 14 for all imaged neurons of a single experiment (one culture of hippocampal neurons from one $Ccp1^{flox/flox}Ccp6^{flox/flox}$ mouse). Pool data from all neurons of a single experiment (separately for control and hyperglutamylated neurons) **(Figs. 1, 3)**.

16. Use Prism or equivalent software to plot scatter dot plots for obtained parameters (run speed, run length and run duration) of all the runs and compare the medians of the respective distributions between control vs. hyperglutamylated neurons for anterograde and retrograde movements **(Figs. 2, 4b-e)**. Exclude displacements of less

than 0.9 µm (average size of a mitochondrion, corresponding to 5 pixels in our system). **See Note 15**.

17. To measure the overall motility of the particles, determine the time all imaged particles in one axon spend in movement within the imaging period using the following equation:

$$Overall\ motility\ [\%] = \frac{Sum\ of\ all\ run\ durations\ in\ the\ kymograph\ [s]\ \times\ 100}{Total\ number\ of\ particles\ \times\ Imaging\ time\ [s]}$$

18. Repeat the experiments (starting with cell cultures from independent mice) and analyses at least five times **(Fig. 1)**.

19. Finally, calculate the 'average run length' and 'average run speed' by calculating the mean of the medians (obtained in step 15) of all experiments **(Figs. 1, 4b-e)**. Calculate the p-values using an unpaired t-test, or another appropriate statistical method, to determine to which extend the differences between control and knockout conditions are statistically significant.

20. Calculate the 'average overall motility' and 'average vesicle density' from all the experiments by calculating the mean of the respective values (obtained in step 17) from all the experiments **(Figs. 1, 4f-i)**. Calculate the p-values using an unpaired t-test, or another appropriate statistical method, to determine to which extend the differences between control and knockout conditions are statistically significant.

4. Notes

1. It is crucial to control the atmosphere of the imaging chamber as it might affect the axonal transport. If CO2-testing equipment is not available, observe the colour of the cell culture medium. At sufficient CO2 levels, it should be between orange and red colour, whereas too low CO2 levels lead to a rather pink colour.
2. This step of washing the neurons can be skipped if they are not transduced with lentivirus.
3. Using higher concentrations or incubating for longer times with the dye can be deleterious to mitochondria. Thus, perform test experiments to determine a suitable concentration of dye at which a good signal is observed without affecting the dynamics of mitochondria.
4. We prefer to use the 60× over the 100× objective, because it allows to image a larger field without compromising on the resolution. As live-imaging produces a huge amount of data, we set the binning at 2×2 to reduce the size of the images. However, if the camera resolution is not sufficient, we recommend to use 1×1 binning.
5. It is important that neurons are seeded at low density to avoid that axons from different neurons grow on each other, which is what they like to do. See chapter (cite our other method paper) for details about neuron culture and seeding for transport experiments. As a general rule, avoid imaging neurons with ambiguous morphology **(Fig. 2)**.
6. The focus plane of bright-field and fluorescence are often different, therefore always check that the vesicles/mitochondria are in focus before acquiring.
7. The signal from the vesicles reduces during acquisition, especially when imaging at higher frame rates. Thus, when adjusting the laser settings ensure that it is strong enough to allows detecting the cargoes throughout the imaging time. If needed, use a spare dish of neurons to adjust laser settings before starting the actual measurements.
8. The rate of acquisition depends primarily on the transport cargo. For mitochondria, lysosomes and endosomes that undergo fast axonal transport, it is suggested to image at least 3 frames per second. For such high-speed imaging, we recommend to use the 'stream mode' or equivalent settings in which the captured images are temporarily stored in the Random-access memory (RAM) of the computer. Only after the entire imaging is completed (1 min in our case), the images will be saved on the local hard

disk. This avoids any delays in the acquisition, thus allowing to capture each frame with high precision in timing.

9. Alternatively, image stack file can be opened by using 'File > Import > Image Sequence' menu in ImageJ.
10. The values are specific for each microscope, dependent on the objective and the camera installed. Ask your microscope facility manager or calculate the pixel value by using the following formula:

$$Image\ pixel\ size = \frac{Camera\ pixel\ size\ \times\ Binning}{Objective\ maginification\ \times \text{lens magnification}\ \times \text{C mount}}$$

11. Start tracing the axon ~15 µm distal from the cell body to avoid the axon initial segment, where transport is atypical [31,32].
12. For our imaging settings, choosing 'width' as 15 pixels was sufficient to cover the diameter of the axon. This might need to be adapted based on the resolution of the camera installed.
13. If necessary, saved tracings can be loaded on to the kymograph later. This is very useful to modify the tracings later on.
14. For counting the particles, we drew a horizontal line in about the middle of the kymograph (~30 s) and counted all particle crossing **(Fig. 3g)**.
15. Data can be visualized in different ways. For instance, the distribution of individual events (run length or run duration) in defined ranges can be represented in histogram plots. These plots are very useful, especially when you expect changes to occur in a particular speed category. This information might not be immediately visible in the dot plots with medians: It is possible that run length/time change only in a specific parameter category between control and treated neurons.

Fig. 1. Schematic representation of the successive steps of a single transport experiment. Primary *Ccp1*$^{flox/flox}$*Ccp6*$^{flox/flox}$ neurons were transduced with either GFP or GFP-2A-cre lentivirus on DIV0 (0 days in vitro), and analysed at DIV4. Mitochondria (stained by the Mitotracker® dye) movements were recorded for 1 min and their transport parameters were analysed using the KymoToolBox plugin. Run speed, run time, run length and overall motility were extracted and compared between control (GFP) and increased polyglutamylation (GFP-2A-cre) conditions. At least five experiments are necessary to calculate the average values of transport parameters obtained from individual experiments.

Fig. 2. Examples of neuron morphologies and their suitability for analysis. Only neurons with a distinct single axon (longest neurite emerging from the cell body) should be selected for analysis (green arrows). Neurons with ambiguous morphologies such as two axons (red #) or overlapping axons (red *) should not be considered for analyses.

Fig. 3. Flowchart of the analysis paradigm to investigate the impact of differential polyglutamylation on axonal transport. (**a**) Hyperstack created from individual frames of the movie. (**b**) The maximum intensity projection of the mitochondria movements throughout the imaging period. (**c**) Hand-drawn line identifying the longest neurite (the axon) in which mitochondria transport will be analysed. (**d**) Kymograph and kymostack of imaged mitochondria created by the KymoToolBox plugin. (**e**) Hand-drawn trajectories of mitochondria runs in the kymographs. (**f**) Colour-coded trajectories identified from (e) (blue: immotile, green: anterograde, red: retrograde). 0.10 μm/sec threshold is applied for defining immotile particles. File with values of transport parameters of all identified trajectories (table format – can be saved as Excel file). For further analysis, the "Summary" lines highlighted in grey should be discarded, as they refer to trajectories containing several runs. Lines highlighted in yellow give the parameters of single runs and should be used for further analyses. The red box highlights the parameters used for further analysis. (**g**) A horizontal line (yellow) is drawn in the middle of the kymograph and the movement trajectories crossing this line were counted as the number of mitochondria in the analysed axon.

Fig. 4. A representative example of data generated from a mitochondria transport experiments from ref. [14]. (**a**) All colour-coded kymographs of mitochondria movements in neurons with normal (GFP) and increased polyglutamylation (GFP-2A-cre) of a single experiment. Runs are defined as immotile (blue), anterograde (green) or retrograde (red) lines.

(**b**) A scatter dot plot of run-length distributions in different experimental conditions. The median values are shown below the graphs. (**c**) A scatter dot plot of run-speed distributions in different experimental conditions. The median values are shown below the graphs. (**d**) Bar graphs of overall motilities of mitochondria in different experimental conditions. It represents the fraction of time the organelles spent in movement throughout the imaging time. (**e**) Bar graphs of mitochondria densities in analysed neurons. **(f-i)** Bar graphs of mean ± SEM values from seven independent experiments (one experiment: a-e), showing run lengths (**f**), run speeds (**g**), overall motility (**h**) and mitochondria densities (**i**). The fold changes between control and hyperglutamylation conditions are shown below the graphs. Statistical significance was tested using unpaired t test. Green: anterograde movement, red: retrograde movement.

Acknowledgments

This work was supported by the ANR-10-IDEX-0001-02, the LabEx CelTisPhyBio ANR-11-LBX-0038. CJ is supported by the Institut Curie, the French National Research Agency (ANR) awards ANR-12-BSV2-0007 and ANR-17-CE13-0021, the Institut National du Cancer (INCA) grant 2014-PL BIO-11-ICR-1, and the Fondation pour la Recherche Medicale (FRM) grant DEQ20170336756. MMM is supported by the EMBO short-term fellowship ASTF 148-2015 and by the Fondation Vaincre Alzheimer grant FR-16055p, and SB by the FRM grant FDT201805005465.

We thank C. Alberti, E. Belloir, F. Bertrand, V. Dangles-Marie, I. Grandjean, C. Caspersen, H. Hermange, A. Thadal, G. Buhagiar, C. Serieyssol, S. Gadadhar, M. Sittewelle (Institut Curie) for technical assistance. We are grateful to M.-N. Soler, C. Lovo and L. Besse from the PICT-IBiSA@Orsay Imaging Facility of the Institut Curie supported by the ANR through the "Investment for the future" program (France-BioImaging, ANR-10-INSB-04), and to N. Manel (Institut Curie, Paris) for material and advice for the lentivirus production. We would like to thank F. Cordelières (Bordeaux Imaging Center, France) for the KymoToolBox plugin, as well as M. Brill (Technical University Munich, Germany), F. Del Bene, V. Marthiens (Institut Curie) and C. González-Billault (University of Chile, Santiago, Chile) for instructive discussions and advice.

References

1. Vale RD (2003) The molecular motor toolbox for intracellular transport. Cell 112 (4):467-480. doi:S0092867403001119 [pii]

2. Franker MAM, Hoogenraad CC (2013) Microtubule-based transport - basic mechanisms, traffic rules and role in neurological pathogenesis. J Cell Sci 126 (Pt 11):2319-2329. doi:10.1242/jcs.115030

3. Millecamps S, Julien J-P (2013) Axonal transport deficits and neurodegenerative diseases. Nat Rev Neurosci 14 (3):161-176. doi:nrn3380 [pii]10.1038/nrn3380

4. Brady ST, Morfini GA (2017) Regulation of motor proteins, axonal transport deficits and adult-onset neurodegenerative diseases. Neurobiol Dis 105:273-282. doi:S0969-9961(17)30084-0 [pii]10.1016/j.nbd.2017.04.010

5. Kneynsberg A, Combs B, Christensen K, Morfini G, Kanaan NM (2017) Axonal Degeneration in Tauopathies: Disease Relevance and Underlying Mechanisms. Front Neurosci 11:572. doi:10.3389/fnins.2017.00572

6. Janke C (2014) The tubulin code: Molecular components, readout mechanisms, and functions. J Cell Biol 206 (4):461-472. doi:jcb.201406055 [pii]10.1083/jcb.201406055

7. Magiera MM, Singh P, Janke C (2018) SnapShot: Functions of Tubulin Posttranslational Modifications. Cell 173 (6):1552-1552 e1551. doi:S0092-8674(18)30644-5 [pii]10.1016/j.cell.2018.05.032

8. Janke C, Rogowski K, Wloga D, Regnard C, Kajava AV, Strub J-M, Temurak N, van Dijk J, Boucher D, van Dorsselaer A, Suryavanshi S, Gaertig J, Eddé B (2005) Tubulin polyglutamylase enzymes are members of the TTL domain protein family. Science 308 (5729):1758-1762. doi:1113010 [pii]10.1126/science.1113010

9. van Dijk J, Rogowski K, Miro J, Lacroix B, Eddé B, Janke C (2007) A targeted multienzyme mechanism for selective microtubule polyglutamylation. Mol Cell 26 (3):437-448. doi:S1097-2765(07)00248-1 [pii]10.1016/j.molcel.2007.04.012

10. Rogowski K, van Dijk J, Magiera MM, Bosc C, Deloulme J-C, Bosson A, Peris L, Gold ND, Lacroix B, Bosch Grau M, Bec N, Larroque C, Desagher S, Holzer M, Andrieux A, Moutin M-J, Janke C (2010) A family of protein-deglutamylating enzymes associated with neurodegeneration. Cell 143 (4):564-578. doi:S0092-8674(10)01184-0 [pii]10.1016/j.cell.2010.10.014

11. Tort O, Tanco S, Rocha C, Bieche I, Seixas C, Bosc C, Andrieux A, Moutin M-J, Xavier Aviles F, Lorenzo J, Janke C (2014) The cytosolic carboxypeptidases CCP2 and CCP3 catalyze posttranslational removal of acidic amino acids. Mol Biol Cell 25 (19):3017-3027. doi:mbc.E14-06-1072 [pii]10.1091/mbc.E14-06-1072

12. Kimura Y, Tsutsumi K, Konno A, Ikegami K, Hameed S, Kaneko T, Kaplan OI, Teramoto T, Fujiwara M, Ishihara T, Blacque OE, Setou M (2018) Environmental responsiveness of tubulin glutamylation in sensory cilia is regulated by the p38 MAPK pathway. Sci Rep 8 (1):8392. doi:10.1038/s41598-018-26694-w10.1038/s41598-018-26694-w [pii]

13. Ikegami K, Mukai M, Tsuchida J-i, Heier RL, Macgregor GR, Setou M (2006) TTLL7 is a mammalian beta-tubulin polyglutamylase required for growth of MAP2-positive neurites. J Biol Chem 281 (41):30707-30716

14. Magiera MM, Bodakuntla S, Ziak J, Lacomme S, Marques Sousa P, Leboucher S, Hausrat TJ, Bosc C, Andrieux A, Kneussel M, Landry M, Calas A, Balastik M, Janke C (2018) Excessive tubulin polyglutamylation causes neurodegeneration and perturbs neuronal transport. EMBO J 37 (23):e100440. doi:embj.2018100440 [pii]10.15252/embj.2018100440

15. Magiera MM, Singh P, Gadadhar S, Janke C (2018) Tubulin Posttranslational Modifications and Emerging Links to Human Disease. Cell 173 (6):1323-1327. doi:S0092-8674(18)30595-6 [pii]10.1016/j.cell.2018.05.018

16. Ikegami K, Sato S, Nakamura K, Ostrowski LE, Setou M (2010) Tubulin polyglutamylation is essential for airway ciliary function through the regulation of beating asymmetry. Proc Natl Acad Sci U S A 107 (23):10490-10495. doi:1002128107 [pii]10.1073/pnas.1002128107

17. Wu H-Y, Wei P, Morgan JI (2017) Role of Cytosolic Carboxypeptidase 5 in Neuronal Survival and Spermatogenesis. Sci Rep 7:41428. doi:srep41428 [pii]10.1038/srep41428

18. Mullen RJ, Eicher EM, Sidman RL (1976) Purkinje cell degeneration, a new neurological mutation in the mouse. Proc Natl Acad Sci U S A 73 (1):208-212

19. Giordano T, Gadadhar S, Bodakuntla S, Straub J, Leboucher S, Martinez G, Chemlali W, Bosc C, Andrieux A, Bieche I, Arnoult C, Geimer S, Janke C (2019) Loss of the

deglutamylase CCP5 perturbs multiple steps of spermatogenesis and leads to male infertility. J Cell Sci 132 (3):10.1242/jcs.226951. doi:jcs.226951 [pii]10.1242/jcs.226951

20. Konno A, Ikegami K, Konishi Y, Yang H-J, Abe M, Yamazaki M, Sakimura K, Yao I, Shiba K, Inaba K, Setou M (2016) Ttll9-/- mice sperm flagella show shortening of doublet 7, reduction of doublet 5 polyglutamylation and a stall in beating. J Cell Sci 129 (14):2757-2766. doi:jcs.185983 [pii]10.1242/jcs.185983

21. Bosch Grau M, Masson C, Gadadhar S, Rocha C, Tort O, Marques Sousa P, Vacher S, Bieche I, Janke C (2017) Alterations in the balance of tubulin glycylation and glutamylation in photoreceptors leads to retinal degeneration. J Cell Sci 130:938-949. doi:jcs.199091 [pii]10.1242/jcs.199091

22. Gilmore-Hall S, Kuo J, Ward JM, Zahra R, Morrison RS, Perkins G, La Spada AR (2019) CCP1 promotes mitochondrial fusion and motility to prevent Purkinje cell neuron loss in pcd mice. J Cell Biol 218 (1):206-219. doi:jcb.201709028 [pii]10.1083/jcb.201709028

23. Shashi V, Magiera MM, Klein D, Zaki M, Schoch K, Rudnik-Schoneborn S, Norman A, Lopes Abath Neto O, Dusl M, Yuan X, Bartesaghi L, De Marco P, Alfares AA, Marom R, Arold ST, Guzman-Vega FJ, Pena LD, Smith EC, Steinlin M, Babiker MO, Mohassel P, Foley AR, Donkervoort S, Kaur R, Ghosh PS, Stanley V, Musaev D, Nava C, Mignot C, Keren B, Scala M, Tassano E, Picco P, Doneda P, Fiorillo C, Issa MY, Alassiri A, Alahmad A, Gerard A, Liu P, Yang Y, Ertl-Wagner B, Kranz PG, Wentzensen IM, Stucka R, Stong N, Allen AS, Goldstein DB, Schoser B, Rosler KM, Alfadhel M, Capra V, Chrast R, Strom TM, Kamsteeg E-J, Bonnemann CG, Gleeson JG, Martini R, Janke C, Senderek J (2018) Loss of tubulin deglutamylase CCP1 causes infantile-onset neurodegeneration. EMBO J 37 (23):e100540. doi:embj.2018100540 [pii]10.15252/embj.2018100540

24. Sirajuddin M, Rice LM, Vale RD (2014) Regulation of microtubule motors by tubulin isotypes and post-translational modifications. Nat Cell Biol 16 (4):335-344. doi:10.1038/ncb2920

25. Ikegami K, Heier RL, Taruishi M, Takagi H, Mukai M, Shimma S, Taira S, Hatanaka K, Morone N, Yao I, Campbell PK, Yuasa S, Janke C, Macgregor GR, Setou M (2007) Loss of alpha-tubulin polyglutamylation in ROSA22 mice is associated with abnormal targeting of KIF1A and modulated synaptic function. Proc Natl Acad Sci U S A 104 (9):3213–3218. doi:Doi 10.1073/Pnas.0611547104

26. Maas C, Belgardt D, Lee HK, Heisler FF, Lappe-Siefke C, Magiera MM, van Dijk J, Hausrat TJ, Janke C, Kneussel M (2009) Synaptic activation modifies microtubules underlying transport of postsynaptic cargo. Proc Natl Acad Sci U S A 106 (21):8731-8736. doi:0812391106 [pii]10.1073/pnas.0812391106

27. Ghiretti AE, Thies E, Tokito MK, Lin T, Ostap EM, Kneussel M, Holzbaur ELF (2016) Activity-Dependent Regulation of Distinct Transport and Cytoskeletal Remodeling Functions of the Dendritic Kinesin KIF21B. Neuron 92 (4):857-872. doi:S0896-6273(16)30704-8 [pii]10.1016/j.neuron.2016.10.003

28. Olenick MA, Dominguez R, Holzbaur ELF (2019) Dynein activator Hook1 is required for trafficking of BDNF-signaling endosomes in neurons. J Cell Biol 218 (1):220-233. doi:jcb.201805016 [pii]10.1083/jcb.201805016

29. Zala D, Hinckelmann M-V, Yu H, Lyra da Cunha MM, Liot G, Cordelieres FP, Marco S, Saudou F (2013) Vesicular glycolysis provides on-board energy for fast axonal transport. Cell 152 (3):479-491. doi:10.1016/j.cell.2012.12.029

30. Schneider CA, Rasband WS, Eliceiri KW (2012) NIH Image to ImageJ: 25 years of image analysis. Nat Methods 9 (7):671-675

31. Albrecht D, Winterflood CM, Sadeghi M, Tschager T, Noe F, Ewers H (2016) Nanoscopic compartmentalization of membrane protein motion at the axon initial segment. J Cell Biol 215 (1):37-46. doi:jcb.201603108 [pii]10.1083/jcb.201603108

32. Kuijpers M, van de Willige D, Freal A, Chazeau A, Franker MA, Hofenk J, Rodrigues RJC, Kapitein LC, Akhmanova A, Jaarsma D, Hoogenraad CC (2016) Dynein Regulator NDEL1 Controls Polarized Cargo Transport at the Axon Initial Segment. Neuron 89 (3):461-471. doi:S0896-6273(16)00047-7 [pii]10.1016/j.neuron.2016.01.022

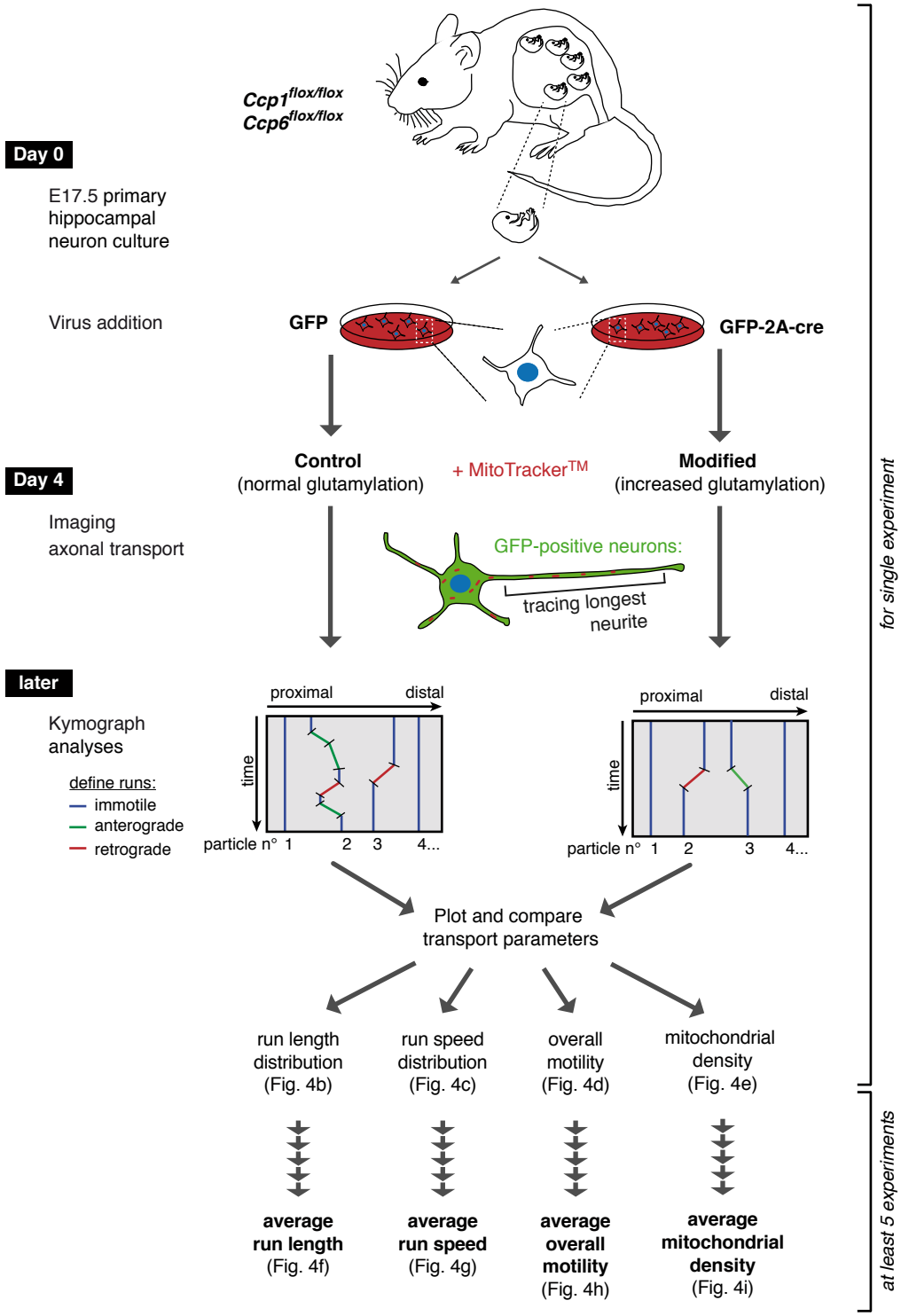
Ccp1flox/flox
Ccp6flox/flox
Day 0
E17.5 primary hippocampal neuron culture
Virus addition
GFP
GFP-2A-cre
Control
(normal glutamylation)
+ MitoTracker™
Modified
(increased glutamylation)
Day 4
Imaging axonal transport
GFP-positive neurons:
tracing longest neurite
later
Kymograph analyses
define runs:
immotile
anterograde
retrograde
proximal
distal
time
particle n° 1 2 3 4...
Plot and compare transport parameters
run length distribution (Fig. 4b)
run speed distribution (Fig. 4c)
overall motility (Fig. 4d)
mitochondrial density (Fig. 4e)
average run length (Fig. 4f)
average run speed (Fig. 4g)
average overall motility (Fig. 4h)
average mitochondrial density (Fig. 4i)
for single experiment
at least 5 experiments

Bodakuntla et al., Figure 2

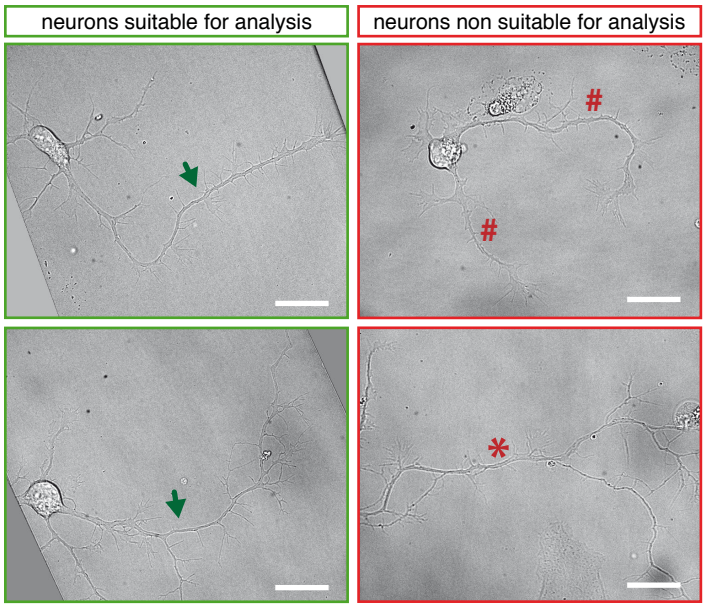

Bodakuntla et al., Figure 3

a

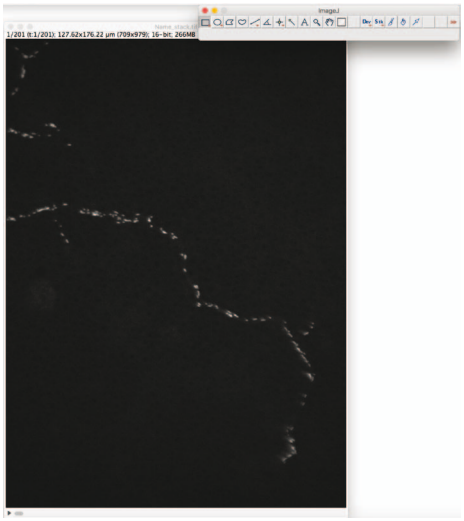

b

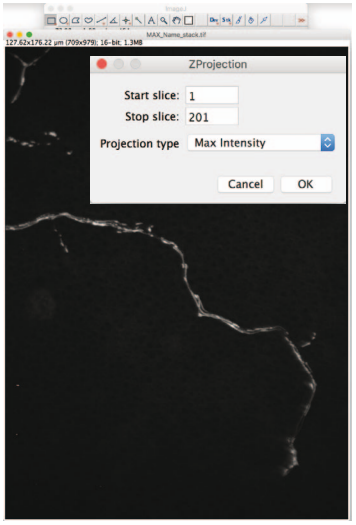

c

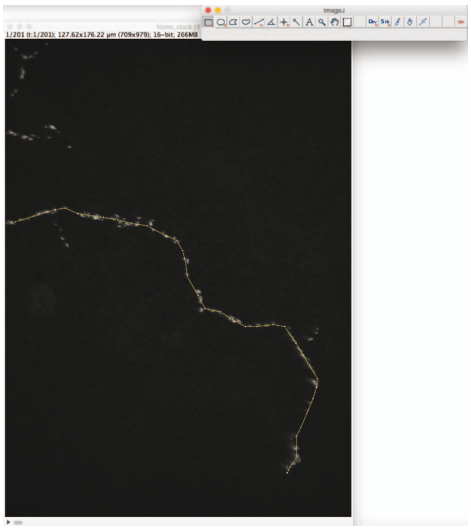

d

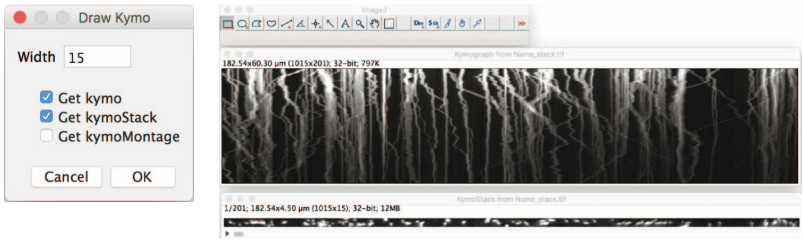

e

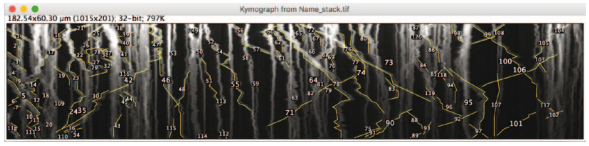

f

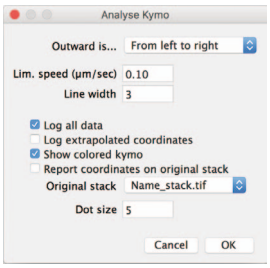

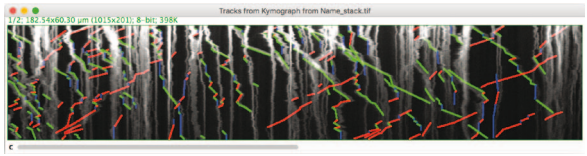

Results

	Label	Kymo_nb	Ttl_Time	Cum_Dist	Mean_Speed	Mean_Speed_In	Mean_Speed_Out	Cum_Dist_In	Cum_Dist_Out	Min_Dist_Start-End	Persistence	Freq_In>Out	Freq_In>Pause	Freq_Out>In	Freq_Out>Pause	Freq_Pause>In	Freq_Pause>Out	%_Ti
1	Kymograph from Name_stack.tif	1	3.300	4.136	1.253	0	0	0	0	0	0	0	0	0	0	0	0	0
2	Kymograph from Name_stack.tif	1	2.700	2.878	1.066	0	0	0	0	0	0	0	0	0	0	0	0	0
3	>>>>Summary for Kymograph from Name_stack.tif<<<<	1	6	7.014	1.169	NaN	1.169	0	7.014	7.014	1	0	0	0	0	0	0	0
4	Kymograph from Name_stack.tif	2	2.400	2.518	1.049	0	0	0	0	0	0	0	0	0	0	0	0	0
5	Kymograph from Name_stack.tif	2	3	0	0	0	0	0	0	0	0	0	0	0	0	0	0	0
6	Kymograph from Name_stack.tif	2	0.300	-0.360	-1.199	0	0	0	0	0	0	0	0	0	0	0	0	0
7	Kymograph from Name_stack.tif	2	3.900	0.180	0.046	0	0	0	0	0	0	0	0	0	0	0	0	0
8	Kymograph from Name_stack.tif	2	0.300	-0.360	-1.199	0	0	0	0	0	0	0	0	0	0	0	0	0
9	>>>>Summary for Kymograph from Name_stack.tif<<<<	2	9.900	3.417	0.345	-1.199	1.049	-0.719	2.518	1.978	1.727	0	0.101	0	0.101	0.202	0	0.06
10	Kymograph from Name_stack.tif	3	0.600	0.899	1.499	0	0	0	0	0	0	0	0	0	0	0	0	0
11	Kymograph from Name_stack.tif	3	1.200	0.180	0.150	0	0	0	0	0	0	0	0	0	0	0	0	0
12	Kymograph from Name_stack.tif	3	2.700	2.878	1.066	0	0	0	0	0	0	0	0	0	0	0	0	0
13	Kymograph from Name_stack.tif	3	1.800	-1.079	-0.599	0	0	0	0	0	0	0	0	0	0	0	0	0
14	Kymograph from Name_stack.tif	3	2.100	1.079	0.514	0	0	0	0	0	0	0	0	0	0	0	0	0
15	Kymograph from Name_stack.tif	3	0	0.899	Infinity	0	0	0	0	0	0	0	0	0	0	0	0	0
16	Kymograph from Name_stack.tif	3	1.800	1.079	0.599	0	0	0	0	0	0	0	0	0	0	0	0	0
17	>>>>Summary for Kymograph from Name_stack.tif<<<<	3	10.200	8.093	0.793	-0.599	0.835	-1.079	7.014	5.935	1.364	0.098	0	0.098	0	0	0	0.17
18	Kymograph from Name_stack.tif	4	1.200	-1.798	-1.499	0	0	0	0	0	0	0	0	0	0	0	0	0
19	>>>>Summary for Kymograph from Name_stack.tif<<<<	4	1.200	1.798	1.499	-1.499	NaN	-1.798	0	1.798	1	0	0	0	0	0	0	1
20	Kymograph from Name_stack.tif	5	1.800	1.798	0.999	0	0	0	0	0	0	0	0	0	0	0	0	0
21	Kymograph from Name_stack.tif	5	5.400	1.978	0.366	0	0	0	0	0	0	0	0	0	0	0	0	0
22	Kymograph from Name_stack.tif	5	1.500	1.619	1.079	0	0	0	0	0	0	0	0	0	0	0	0	0
23	Kymograph from Name_stack.tif	5	1.800	0	0	0	0	0	0	0	0	0	0	0	0	0	0	0
24	Kymograph from Name_stack.tif	5	1.500	1.439	0.959	0	0	0	0	0	0	0	0	0	0	0	0	0

g

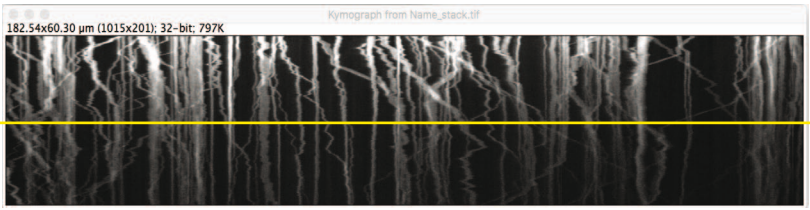

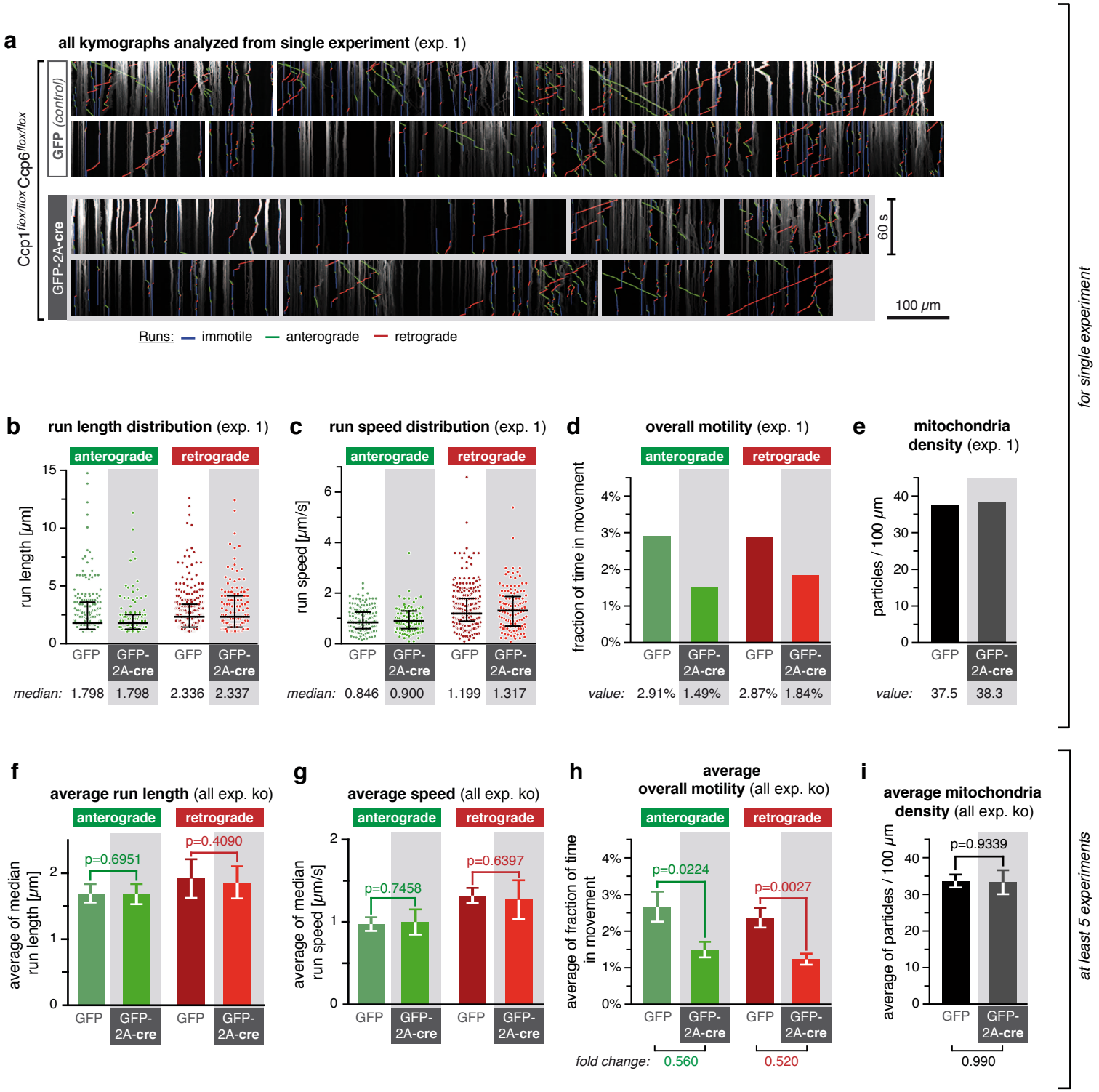
a
all kymographs analyzed from single experiment (exp. 1)
Ccp1flox/flox Ccp6flox/flox
GFP (control)
GFP-2A-cre
60 s
100 µm
Runs: immotile anterograde retrograde
for single experiment
b
run length distribution (exp. 1)
anterograde
retrograde
run length [µm]
GFP
GFP-2A-cre
median: 1.798 1.798 2.336 2.337
c
run speed distribution (exp. 1)
run speed [µm/s]
median: 0.846 0.900 1.199 1.317
d
overall motility (exp. 1)
fraction of time in movement
value: 2.91% 1.49% 2.87% 1.84%
e
mitochondria density (exp. 1)
particles / 100 µm
value: 37.5 38.3
at least 5 experiments
f
average run length (all exp. ko)
average of median run length [µm]
p=0.6951
p=0.4090
g
average speed (all exp. ko)
average of median run speed [µm/s]
p=0.7458
p=0.6397
h
average overall motility (all exp. ko)
average of fraction of time in movement
p=0.0224
p=0.0027
fold change: 0.560 0.520
i
average mitochondria density (all exp. ko)
average of particles / 100 µm
p=0.9339
0.990